

Synthesis of Vertically Aligned Single- and Double-Walled Carbon Nanotubes without Etching Agents

Vijaya Kumar Kayastha, Shun Wu, Jason Moscatello, and Yoke Khin Yap*

Department of Physics, Michigan Technological University, 1400 Townsend Drive, Houghton, Michigan 49931

Received: May 9, 2007; In Final Form: June 6, 2007

The number of graphene shells on carbon nanotubes (CNTs) can be rationally controlled to yield high-density, vertically aligned single- and double-walled CNTs. This was obtained by thermal chemical vapor deposition at 700 °C without the use of etching agents such as water, oxygen, or plasma. The key factors for this success are controlled dissociative adsorption of acetylene (C₂H₂) molecules and subnanometer thickness control of the Al/Fe/Mo trilayer films. We propose that an Al concave meniscus confines the actual growth surface areas of Fe/Mo catalytic nanoparticles and enables the control of the number of graphene shells on CNTs.

Structural and electronic properties of single-walled carbon nanotubes (SWCNTs) are attractive for applications such as nanoelectronic devices^{1–3} and chemical and biological sensors.^{4,5} On the other hand, double-walled carbon nanotubes (DWCNTs) have recently gained attentions for their relatively more stable thermal and structural properties than those of SWCNTs.^{6,7} Despite these promises, the effective growth of SWCNTs and DWCNTs with the desired number of graphene shells is challenging. The most effective growth mode requires that most of the catalysts on the substrates remain active and lead to the growth of high-density, vertically aligned (VA) nanotubes. This optimum growth mode is now achievable for multiwalled carbon nanotubes by conventional thermal chemical vapor deposition (CVD).^{8–11} However, the understanding on growing VA-SWCNTs and VA-DWCNTs by thermal CVD is still at the infancy.

Most reported SWCNTs and DWCNTs were grown at high temperatures (~1000 °C) in a random form.^{12,13} Murakami et al. demonstrated the growth of VA-SWCNTs at 800 °C by using ethanol as the source gas.¹⁴ VA-SWCNTs were also obtained by using plasma-enhanced chemical vapor deposition (PECVD) techniques.^{15,16} Recently, VA-SWCNTs were grown at 750 °C by a water-assisted thermal CVD technique using ethylene as the source gas.¹⁷ Dai et al. reported the growth of VA-SWCNTs at 720 °C by oxygen-assisted inductively coupled radio frequency PECVD using methane as the source gas.¹⁸ All of these techniques involved the use of plasma, oxygen, or water, which have etching and oxidation effects.

Here, we report the control of a number of graphene shells on CNTs at 700 °C without the use of etching agents. This has led to the growth of VA-SWCNTs and VA-DWCNTs simply by conventional thermal CVD. Our experiments were guided by the molecular dynamics of the dissociative adsorption of acetylene (C₂H₂) molecules on an Fe catalyst.¹⁹ Our growth model suggests that the decomposition rate must be controlled

to achieve equilibrium with the rates of the subsequent carbon diffusion into the catalysts and the carbon segregation from the catalysts.

We have chosen to use Al/Fe/Mo trilayer catalyst films,²⁰ which are effective for the growth of SWCNTs. We first tested the functions of Fe, Mo, and Al in the trilayer catalyst films. We used pulsed-laser deposition⁸ to coat (i) Fe, (ii) Fe/Mo (Mo on Fe), (iii) Al/Fe (Fe on Al), and (iv) Al/Fe/Mo (Mo on Fe on Al) films on oxidized Si substrates. The thicknesses of Al, Fe, and Mo were 10, 0.5, and 0.1 nm, respectively. The catalyst-coated substrates were annealed in the quartz tube chamber of our thermal CVD system at 700 °C in the flow of H₂ gas for 10 min to create catalyst particles. This was followed by a 1 h growth using acetylene and H₂ gas (C₂H₂ = 3 sccm and H₂ = 120 sccm).

Figure 1 shows Raman spectra and corresponding scanning electron microscopy (SEM) images (insets) of the CNT films grown by different catalyst films. As shown in Figure 1a, the sample grown by the Fe catalyst does not indicate the disorder (D) and the graphitic (G) peaks, which correspond to the K-point phonons of A_{1g} symmetry and the zone center phonons of E_{2g} symmetry of graphite, respectively.^{8,19} This is due to the fact that very few short MWCNTs were grown, as shown in the inset. When Fe/Mo films were used for the growth, both D and G peaks were detected, as shown in Figure 1b. This is due to the increase of nanotube density and length, as shown in the inset. This result indicates that Fe/Mo is relatively more effective for the growth of CNTs at 700 °C. It is interesting to detect D and G peaks as well as the radial breathing mode (RBM) of SWCNTs from a sample grown by Al/Fe catalysts (Figure 1c). The density of CNTs has increased (inset) and is dominated by SWCNTs, as indicated by a relatively intense G peak and the shoulder at the lower frequency of the G peak. This means that the Al underlayer has facilitated the Fe catalyst for the growth of SWCNTs. The best result was obtained when the Al/Fe/Mo trilayer films were used, as shown in Figure 1d. Denser

* To whom correspondence should be addressed. E-mail: ykyap@mtu.edu.

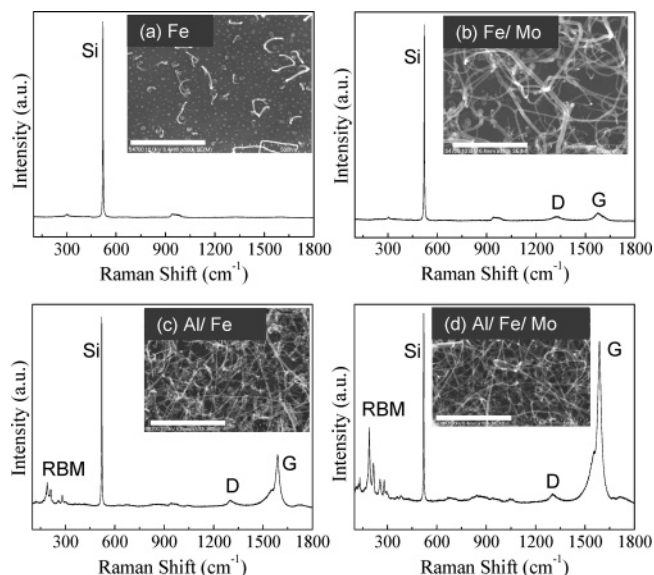


Figure 1. Raman spectra (laser excitation wavelength is 632 nm) and corresponding SEM images (insets) of CNTs grown by using (a) Fe, (b) Fe/Mo, (c) Al/Fe, and (d) Al/Fe/Mo catalysts. Scale bars are 500 nm.

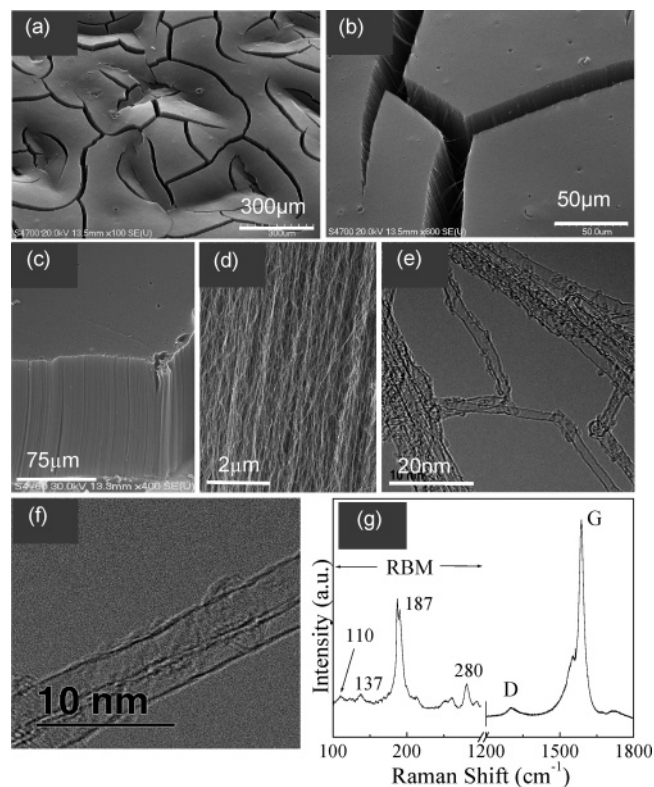


Figure 2. Images of VA-SWCNTs. (a–d) SEM images taken at different magnifications at a tilted angle of 45°, (e–f) HRTEM images showing bundles of SWCNTs, and (g) Raman spectrum of the corresponding SWCNT film (laser excitation wavelength is 632 nm).

SWCNTs were grown (inset) with a stronger and sharper RBM and G peaks.

As guided by our growth model, we have systematically increased the flow of the acetylene gas, which leads to the growth of high-density SWCNTs at 10 sccm, as shown in Figure 2a–d. The density of these SWCNTs is high and leads to the appearance of a smooth-top surface at low magnification. Cracking is observed from this sample, as also observed on other high-density SWCNTs, probably due to mechanical and thermal

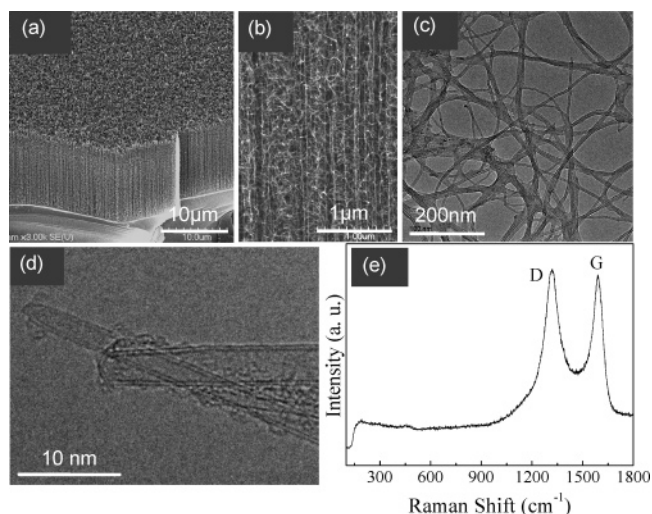


Figure 3. Images of high-density vertically aligned DWCNTs. SEM images were taken at a tilted angle of 45° with (a) low and (b) high magnification. TEM images at (c) low and (d) high magnification. (e) Raman spectrum of a DWCNT film (laser excitation wavelength is 632 nm).

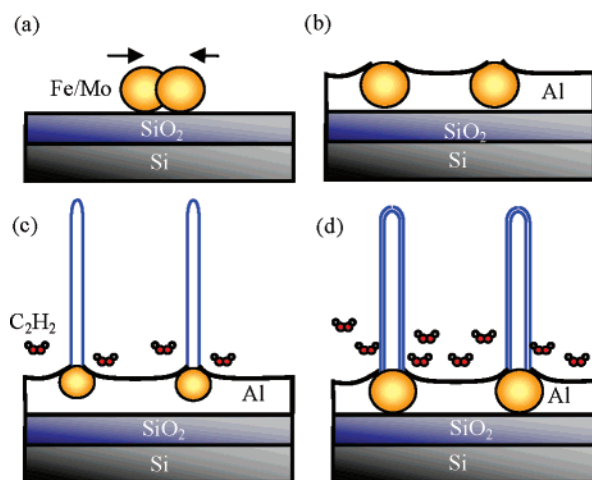


Figure 4. Conceptual diagrams showing (a) diffusion and sintering of Fe/Mo nanoparticles on oxidized Si substrates, (b) sinking of the Fe/Mo nanoparticles into the Al melt, and the growth of (c) VA-SWCNTs or (d) VA-DWCNTs at optimum supplies of acetylene source gas and appropriate sizes of Fe/Mo nanoparticles.

stress during the growth and the handling processes.^{15,16} The length of these SWCNTs is $\sim 170 \mu\text{m}$ as grown in 10 min. Transmission electron microscopy (TEM) indicates that some SWCNTs can be as large as $\sim 2.3 \text{ nm}$ in diameter, as shown in Figure 2e and f. TEM sampling indicates that these are 100% of the SWCNTs without an observable trace catalyst. We believe that the growth of these SWCNTs follows the base growth mode and that all of the catalysts remain on the substrate surface. This is confirmed by the inspection of the SEM after the scratching of some SWCNTs from the substrate. Raman spectra in Figure 2g show intense RBM peaks and the split G peak of SWCNTs. The diameters of these SWCNTs are calculated as $\sim 0.9, 1.33, 1.8,$ and 2.25 nm by using the relation $\omega \text{ (cm}^{-1}\text{)} = 248/d \text{ (nm)}$, where ω is the wavenumber of the Raman shifts and d is the diameter of the nanotubes.²¹

We have explored controlling the number of graphene shells on the nanotubes. We have first doubled the thickness of the Fe and Mo films, that is, using Al, Fe, and Mo films of 10, 1.0, and 0.2 nm, respectively. It is known that DWCNTs require thicker catalyst films than those needed for the growth of

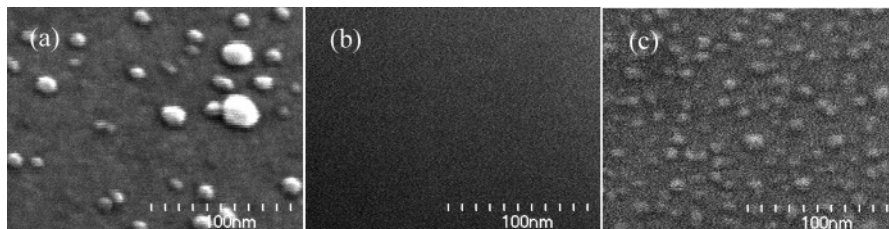


Figure 5. Representative appearances of a (a) Fe/Mo film, (b) Al film, (c) Al/Fe/Mo film after the pretreatment process. All of these films were coated on oxidized Si substrates.

SWCNTs.²² Then, we increased the supply of acetylene systematically from 10 to 50 sccm to accommodate the growth of the additional graphene shell. By this approach, VA-DWCNTs were successfully grown, as shown in Figure 3a and b. These VA-DWCNTs could be grown as long as 16 μm long in 1 min. TEM images of these DWCNTs are shown in Figure 3c and d. As estimated by TEM, these samples contained more than 80% of DWCNTs, with some SWCNTs and MWCNTs. The diameters of these DWCNTs can be as large as ~ 4 nm, with possible RBM signals at a Raman shift < 70 cm^{-1} , which are beyond the detection limit of the spectrometer (cutoff ~ 100 cm^{-1}), as shown in Figure 3e. RBM signals at higher Raman shifts were also not detected due to the small contents of SWCNTs. Amorphous carbon was detected at the sidewalls of these DWCNTs. These could have contributed to a strong D peak as compared to that in SWCNTs.

There are two major factors for the controlled growth of VA-SWCNTs and VA-DWCNTs at relatively low temperatures. The first factor is the effective Al/Fe/Mo catalysts. The second factor is the controlled dissociative adsorption of acetylene molecules.¹⁹ The controlled supplies of the hydrocarbon molecules are important,²³ otherwise this will lead to random SWCNTs^{12,20} or multiwalled nanotubes,²⁴ even when Al/Fe/Mo catalysts are used. The exothermic process can also create higher temperatures near the catalyst surfaces and supply the formation energy for folding small curvature graphene shells.

The use of Fe or Fe/Mo catalysts alone cannot form small catalytic particles for SWCNTs and DWCNTs due to the aggregation of nanoparticles (Figure 4a). The results in Figure 1 indicate that the Al underlayer plays some important roles for growing SWCNTs. Al has a relatively low melting point (660.37 $^{\circ}\text{C}$). Since the density of Fe (7.86 g/cm^3 at 293 K) and Mo (10.22 g/cm^3 at 293 K) are higher than that of Al (2.702 g/cm^3 at 293 K),^{25,26} Al will remain as a liquid layer and cause the Fe/Mo nanoparticles to sink into the melts, as shown in Figure 4b. Since the cohesive energy of Al–Al bonds (3.39 eV/atom) is lower than the cohesive energies of Fe–Fe (4.28 eV/atom) and Mo–Mo (6.82 eV/atom),²³ capillary activity will cause Al liquid to form a concave meniscus around the Fe/Mo nanoparticles, as shown in Figure 4. In this way, the actual area of the catalysts that is exposed for the growth of CNTs is smaller and thus enables the growth of SWCNTs (Figure 4c). In addition, Al could have increased the resistance against surface diffusion of the Fe/Mo nanoparticles and prevented sintering. Larger Fe/Mo particles can be formed with thicker Fe/Mo films. At an optimum film thickness, appropriate areas of the Fe/Mo nanoparticles will be exposed to the acetylene molecules for the growth of DWCNTs (Figure 4d). We cannot exclude the presence of oxides (including Al_xO_y)¹² in the catalyst films. However, since our samples are pretreated and grown in the flow of H_2 gas, the contribution of oxides should be minimum.

To supplement our discussion on the function of the trilayer catalyst, a series of catalyst films have been annealed at

700 $^{\circ}\text{C}$ in the flow of H_2 gas for 10 min, as outlined in the pretreatment process described earlier. These samples were then cooled to room temperature in the flow of H_2 gas. The surface morphologies of these samples were then examined by SEM and are shown in Figure 5a, b, and c for (i) Fe/Mo (Mo on Fe), (ii) Al, and (iii) Al/Fe/Mo (Mo on Fe on Al) films, respectively. The thickness of the Al, Fe, and Mo films were 10, 0.5, and 0.1 nm, respectively. As shown in Figure 5a, the Fe/Mo film coated on an oxidized Si substrate has transformed into spherical nanoparticles with diameters of 10–30 nm, consistent with that illustrated in Figure 4a. The 10 nm thick Al film appears to form a smooth thin film after the annealing, as shown in Figure 5b. The Fe/Mo film coated on a 10 nm thick Al film has formed nanoparticles of ~ 10 –15 nm, as shown in Figure 5c. The appearance of these nanoparticles is different as compared to those in the case in Figure 5a. We interpret this appearance as spherical nanoparticles that are partially sunk into the Al film. We believed that the surfaces of these Fe/Mo particles are partially coated with Al due to the concave meniscus formed by the capillary activity discussed earlier. Thus, the actual Fe/Mo catalyst surfaces exposed for the growth of CNTs are smaller than that indicated by their diameters. Since Fe is also a good catalyst for the growth of boron nitride nanotubes (BNNTs)²⁷ and the dimensions of the catalyst particles have been shown to control the diameters of boron–carbon nitride (BCN) nanotubes,²⁸ we think that the use of the Al/Fe/Mo films discussed here could be useful for the growth of BNNTs and BCN nanotubes.

In summary, rational control of the number of graphene shells on CNTs was obtained at 700 $^{\circ}\text{C}$ by conventional thermal CVD. Both an optimum flow rate of acetylene gas and Al/Fe/Mo trilayer catalysts are important for the growth of these VA-SWCNTs and VA-DWCNTs. This result indicates that further understanding of the dissociative adsorption of acetylene molecules and the functions of the trilayer catalyst is important for the effective growth of SWCNTs and DWCNTs at low temperatures.

Acknowledgment. We acknowledge support from the U.S. Department of Army (Grant No. W911NF-04-1-0029, through the City College of New York), Defense Advanced Research Agency (Contract No. DAAD17-03-C-0115, through Army Research Laboratory), and the Center for Nanophase Materials Sciences sponsored by the Division of Materials Sciences and Engineering, U.S. Department of Energy (Contract No. DE-AC05-00OR22725 with UT–Battelle, LLC.).

References and Notes

- (1) Tans, S. J.; Verschuere, A. R. M.; Dekker, C. *Nature* **1998**, *391*, 60.
- (2) Odom, T. W.; Huang, J.; Kim, P.; Lieber, C. M. *Nature* **1998**, *391*, 62.
- (3) Martel, R.; Schmidt, T.; Shea, H. R.; Hertel, T.; Avouris, P. *Appl. Phys. Lett.* **1998**, *73*, 2447.
- (4) Kong, J.; Franklin, N. R.; Zhou, C.; Chapline, M. G.; Peng, S.; Cho, K.; Dai, H. *Science* **2000**, *287*, 622.

- (5) Collins, P. G.; Bradley, K.; Ishigami, M.; Zettl, A. *Science* **2000**, *287*, 1801.
- (6) Endo, M.; Muramatsu, H.; Hayashi, T.; Kim, Y.; Lier, G. V.; Charlier, J. C.; Terrones, H.; Terrones, M.; Dresselhaus, M. S. *Nano Lett.* **2005**, *5*, 1099.
- (7) Endo, M. H.; Hayashi, T.; Kim, Y. A.; Terrones, M.; Dresselhaus, M. S. *Nature* **2005**, *433*, 476.
- (8) Kayastha, V. K.; Yap, Y. K.; Pan, Z.; Ivanov, I. N.; Puzos, A. A.; Geohegan, D. B. *Appl. Phys. Lett.* **2005**, *86*, 253105.
- (9) Pinault, M.; Pichot, V.; Khodja, H.; Launois, P.; Reynaud, C.; L'Hermite, M. M. *Nano Lett.* **2005**, *5*, 2394.
- (10) Li, X.; Cao, A.; Jung, Y. J.; Vajtai, R.; Ajayan, P. M. *Nano Lett.* **2005**, *5*, 1997.
- (11) Xiong, G. Y.; Wang, D. Z.; Ren, Z. F. *Carbon* **2006**, *44*, 969.
- (12) Lacerda, R. G.; Teo, K. B. K.; Teh, A. S.; Yang, M. H.; Dalal, S. H.; Jefferson, D. A.; Durrell, J. H.; Rupasinghe, N. L.; Roy, D.; Amaratunga, G. A. J.; Milne, W. I.; Wycisk, F.; Legagneux, P.; Chhowalla, M. *J. Appl. Phys.* **2004**, *96*, 4456.
- (13) Lee, Y. D.; Lee, H. J.; Han, J. H.; Yoo, J. E.; Lee, Y.-H.; Kim, J. K.; Nahm, S.; Ju, B.-K. *J. Phys. Chem. B* **2006**, *110*, 5310.
- (14) Murakami, Y.; Chiashi, S.; Miyauchi, Y.; Hu, M.; Ogura, M.; Okubo, T.; Maruyama, S. *Chem. Phys. Lett.* **2004**, *385*, 298.
- (15) Zhong, G.; Iwasaki, T.; Honda, K.; Furukawa, Y.; Ohdomari, I.; Kawarada, H. *Jpn. J. Appl. Phys.* **2005**, *44*, 1558.
- (16) Wang, Y. Y.; Gupta, S.; Nemanich, J. *Appl. Phys. Lett.* **2004**, *85*, 2601.
- (17) Hata, K.; Futaba, D. N.; Mizuno, K.; Namai, T.; Yumura, M.; Iijima, S. *Science* **2004**, *306*, 1362.
- (18) Zhang, G.; Mann, D.; Zhang, L.; Javey, A.; Li, Y.; Yenilmez, E.; Wang, Q.; McVittie, J. P.; Nishi, O.; Gibbons, J.; Dai, H. *Proc. Natl. Acad. Sci. U.S.A.* **2005**, *102*, 16141.
- (19) Kayastha, V. K.; Yap, Y. K.; Dimovski, S.; Gogotsi, Y. *Appl. Phys. Lett.* **2004**, *85*, 3265.
- (20) Delzeit, L.; Chen, B.; Cassel, A.; Stevens, R.; Nguyen, C.; Meyyappan, M. *Chem. Phys. Lett.* **2001**, *348*, 368.
- (21) Jorio, A.; Saito, R.; Hafner, J. H.; Lieber, C. M.; Hunter, M.; McClure, T.; Dresselhaus, G.; Dresselhaus, M. S. *Phys. Rev. Lett.* **2001**, *86*, 1118.
- (22) Yamada, T.; Namai, T.; Hata, K.; Futaba, D.; Mizuno, K.; Fan, J.; Yudasaka, M.; Yumura, M.; Iijima, S. *Nat. Nanotechnol.* **2006**, *1*, 131.
- (23) Cui, H.; Eres, G.; Howe, J. Y.; Puzos, A.; Varela, M.; Geohegan, D. B.; Lowndes, D. H. *Chem. Phys. Lett.* **2003**, *374*, 222.
- (24) Geohegan, D. B.; Puzos, A. A.; Ivanov, I.; Jesse, S.; Eres, G.; Howe, J. Y. *Appl. Phys. Lett.* **2003**, *83*, 1851.
- (25) Pearson, W. B. *Crystal Chemistry and Physics of Metals and Alloys*; Wiley: New York, 1972.
- (26) Kittel, C. *Introduction to Solid State Physics*, 6th ed.; Wiley: New York, 1986.
- (27) Wang, J.; Kayastha, V.; Yap, Y. K.; Fan, Z.; Lu, J. G.; Pan, Z.; Ivanov, I.; Puzos, A. A.; Geohegan, D. B. *Nano Lett.* **2005**, *5*, 2528.
- (28) Wang, W. L.; Bai, X. D.; Liu, K. H.; Xu, Z.; Golberg, D.; Bando, Y.; Wang, E. G. *J. Am. Chem. Soc.* **2006**, *128*, 6530.